Metrol. Meas. Syst., Vol. 30 (2023) No. 1, pp. 83–97
DOI: 10.24425/mms.2023.144394

PAN POLSKA AKADEMIA NAUK

METROLOGY AND MEASUREMENT SYSTEMS
Index 330930, ISSN 0860-8229
www.metrology.wat.edu.pl

M&MS

AN INTELLIGENT COMPOUND GEAR-BEARING FAULT IDENTIFICATION APPROACH USING BESSEL KERNEL-BASED TIME-FREQUENCY DISTRIBUTION

Athisayam Andrews, Kondal Manisekar

Department of Mechanical Engineering, National Engineering College, Kovilpatti, Tamilnadu, India
(*andrewsnzt@gmail.com*, *kmsekar1@rediffmail.com*)

Abstract

The most crucial transmission components utilized in rotating machinery are gears and bearings. In a gearbox, the bearings support the force acting on the gears. Compound Faults in both the gears and bearings may cause heavy vibration and lead to early failure of components. Despite their importance, these compound faults are rarely studied since the vibration signals of the compound fault system are strongly dominated by noise. This work proposes an intelligent approach to fault identification of a compound gear-bearing system using a novel Bessel kernel-based Time-Frequency Distribution (TFD) called the Bessel transform. The Time-frequency images extracted using the Bessel transform are used as an input to the Convolutional Neural Network (CNN), which classifies the faults. The effectiveness of the proposed approach is validated with a case study, and a testing efficiency of 94% is achieved. Further, the proposed method is compared with the other TFDs and found to be effective.

Keywords: compound gear-bearing faults, Bessel transform, time-frequency distribution, convolutional neural network.

1. Introduction

Rotating machinery contains various components that are prone to failure; nevertheless, gears and bearings are the most common locations of defects. As a result, accurate identification of the early phases of these components' defects has recently received much attention. Vibration-based fault diagnosis is a proven technique for early identification of gear and bearing defects [1,2]. The three principal vibration-based fault diagnosis approaches are the time domain, frequency domain, and time-frequency domain. Defective bearings and gears often produce nonstationary signals because of their fluctuating frequency. The scarcity of information in the time and frequency domains made recognizing defects with time and frequency domain analysis more complex. On the other hand, the *time-frequency distribution* (TFD) blends both the time and frequency information [3]. Many studies on vibration-based fault diagnosis of gears and bearings have been conducted.

Article history: received September 9, 2022; revised September 29, 2022; accepted September 29, 2022; available online December 28, 2022.

Short-time Fourier Transform (STFT) [4, 5], *Wigner-Ville Distribution* (WVD) [6], *Discrete Wavelet Transform* (DWT) [7,8], and *Continuous Wavelet Transform* (CWT) [9,10] are commonly used to convert the time domain signal into the time-frequency distribution. However, these methods have their drawbacks. The performance of the STFT depends on the type and length of the window. The time-frequency bins are linearly spaced and have a consistent time and frequency resolution in STFT. In contrast, the *constant-Q transform* (CQT) offers a frequency resolution that depends on the analysis windows' centre frequencies being spatially separated geometrically [11]. The WVD generates cross terms, which affects its fault identification potential [7, 12]. The DWT suffers from shift sensitivity and poor directionality [13]. Cohen proposed a generalized model of the phase-space distribution, and all other time-frequency distributions can be derived from this [12]. The performance distribution is improved by selecting the suitable time kernel based on its application. Satish Rajagopalan *et al.* [12] have proposed a new kernel in Cohen's phase-space distribution to suppress the cross-terms time-frequency transform called the *Zhao-Atlas-Marks* transform (ZAM) [14]. Zhenyu Guo *et al.* [15] suggested a novel TFD termed the *Bessel distribution* (BD) employing a Bessel function-based kernel. This kernel suppresses the cross-terms, which improves time-frequency resolution to analyse nonstationary signals effectively.

Many deep learning approaches have been used to classify the TFD images and identify the faults. Based on the provided dataset, deep learning techniques can automatically extract the features [16]. To achieve this, researchers used various deep learning techniques. Sai Ma *et al.* [17] used a deep residual network for fault diagnosis of a planetary gearbox running under nonstationary conditions. Li-Hua Wang *et al.* [18] used a *Convolutional Neural Network* (CNN) along with STFT for fault identification in motors. Iskander Imed Eddine Amarouayache *et al.* [19] used CNN for fault diagnosis of bearings. Yahui Zhang *et al.* [20] applied a *Recurrent Neural Network* (RNN) for the fault classification of a CWRU bearing dataset. Yingkui Gu *et al.* [21] used a Deep *Convolutional Neural Network* (DCNN) along with signal denoising to effectively identify bearing faults. Among that, CNN has been proven to be effective for image recognition problems [22–24]. Wei Zhang *et al.* [25] suggested that the efficiency of the CNN can be increased by increasing the amount of data through data augmentation.

Compound faults are still complicated since the multiple systems' vibration signals are merged. Haidong Shao *et al.* [26] proposed an adaptive dual-tree complex wavelet packet transform in the compound fault diagnosis. Laxmikant S. Dhamande and Mangesh B. Chaudhari [27] compared the performance of a Continuous Wavelet Transform with a Discrete Wavelet Transform along with statistical features using an *Artificial Neural Network* (ANN) as the classifier in compound fault identification. They also evaluated the performance of time-frequency domain features as compared to those of time and frequency domains s and discovered that time-frequency domain features are more effective. Lu Ou and Dejie Yu [28] used a graph Fourier transform-based extraction technique to identify compound faults. Ali Dibaj *et al.* [29] and Juan Xu *et al.* [30] utilized a *convolutional neural network* (CNN) as a classifier for identifying compound defects. Ruyi Huang *et al.* [31] proposed a deep capsule network and ensemble learning for compound defects. Ruyi Huang *et al.* [32] proposed a Deep Decoupling Convolutional Neural Network for decoupling the compound faults. A deep transfer learning method called transferable capsule network is employed by Ruyi Huang *et al.* [33]. Ruyi Huang *et al.* [34] also proposed a deep adversarial capsule network to further improve compound defects' classification potential. Lingli Cui *et al.* [35] introduced an adapted dictionary-free orthogonal matching pursuit and 0-1 programming for compound gear-bearing fault identification. Baihong Zhong *et al.* [36] developed a deep progressive shrinkage learning method for identifying compound faults with intense background noise. Prasad V. Shinde and Ramchandra G. Desavale [37] combined a matrix method of dimensional analysis with a *support vector machine* (SVM) to investigate unbalance

Metrol. Meas. Syst., Vol. 30 (2023), No. 1, pp. 83–97
DOI: 10.24425/mms.2023.144394

and misalignment present in the system. To effectively identify the compound faults, a durable TFD transform and feature selection are required to obtain trustworthy information about the faults.

The more complicated but actual situation of compound gear-bearing faults is considered in this work. This is a severe condition that will lead to the system failing sooner than single or multiple emerging faults in individual components. This work proposes a novel TFD transform using the Bessel kernel to obtain the time-frequency domain signals to identify compound gear-bearing faults effectively. The effectiveness of the time-frequency transformation is then tested by employing a fine-tuned CNN as a classifier. Further, the effectiveness of the proposed Bessel transform-based fault identification is compared with the CWT, CQT and *Smoothed-pseudo WVD* (SPWVD) transform-based fault identification. The results show that the proposed Bessel TFD transform outperforms traditional TFD transforms.

The rest of this paper is organized as follows. Section 2 explains the methods proposed in this paper. Section 3 discusses the experimental studies carried out. Section 4 analyses the proposed method's performance and compares it to the CWT, CQT and SPWVD transform-based approaches. The results show that the proposed Bessel transform-based fault identification method is more effective in detecting compound gear-bearing faults. Conclusions are given in Section 5.

2. Proposed methodology

The proposed approach to identifying compound gear-bearing defects using Time-Frequency domain analysis is shown in Fig. 1. At first, vibration signals are acquired from a data acquisition system. Then the signals are converted into TFD using the Bessel transform. Finally, the CNN is enforced to classify the TFD images to identify the fault conditions of the system. The various stages of the proposed fault identification method are detailed below.

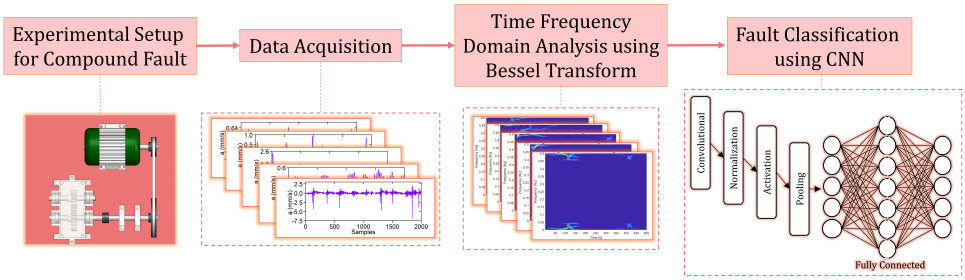

Fig. 1. Proposed methodology.

2.1. Time-frequency domain analysis using Bessel transform

This work proposes a novel time-frequency domain called the Bessel transform to convert the time domain vibration signals into TFD. The Bessel transform has evolved by implementing a Bessel function-based kernel in Cohen's class distribution. The Bessel kernel handles non-stationary signals effectively by achieving high time-frequency resolution and eliminating cross terms. The general form of Cohen's class of distributions is given in (1) [38]. The time signal is

represented by $f(\mu)$, and its complex conjugate is $f^*(\mu)$.

$$C(t,\omega,\Phi) = \frac{1}{2\pi}\iiint e^{j(\xi\mu-\tau\omega-\xi t)}\Phi(\xi,\tau)f\left(\mu+\frac{\tau}{2}\right)f^*\left(\mu-\frac{\tau}{2}\right)\mathrm{d}\mu\,\mathrm{d}\tau\,\mathrm{d}\xi, \tag{1}$$

where ω – instantaneous frequency, t – instantaneous time, τ – running time, ξ – frequency, μ – position variables employed in the integration, and $\Phi(\xi,\tau)$ – kernel deciding on the distribution.

The Bessel distribution is obtained by substituting the Bessel kernel in Cohen's distribution class [15]. The Bessel kernel is given by

$$\Phi(\xi,\tau) = \frac{J_1(2\pi\alpha\xi\tau)}{\pi\alpha\xi\tau}, \tag{2}$$

where J_1 – a first kind Bessel function, α – a scaling factor greater than 0.

2.2. Fault classification using CNN

CNN is a deep neural network distinguished by the structure of neurons with trainable weights and biases. Researchers have created many CNN architectures for applications like shape identification, image processing, and video analysis. Each CNN comprises a set of convolution layers, batch normalization layer, activation layer, pooling layer and fully connected layers. Each layer in the CNN is explored briefly below.

2.2.1. Convolutional layer

As an input to the following layer, the convolutional layer convolves the input feature map using learnable convolutional kernels to produce several new feature maps. The activation function obtains the output after convolutional processes [19].

In general, the following equation can describe the mathematical model of the convolutional layer.

$$x_j^l = f\left(\sum_{i\in M_j} x_i^{l-1} * k_{ij}^l + b_j^l\right) \tag{3}$$

where x_j^l indicates the l-th feature in the j-th layer, * denotes the convolution operation, M are the input features, k is the convolution kernel, b is the bias term, and f is the non-linear activation function.

2.2.2. Batch normalization layer

The batch normalization layer is intended to diminish internal covariance shift and quicken deep neural network training. Typically, this layer is introduced just before the activation unit and follows the convolutional or fully-connected layer. The conversion of the batch normalization layer is stated as follows:

$$k_i = \frac{x_i - \mu}{\sqrt{\sigma^2+\epsilon}} \tag{4}$$

and

$$y_i = \gamma k_i + \beta, \tag{5}$$

where, y_i is the output of each neuron, γ and β are scale and shift coefficients, μ and σ represent the mean and variance of the samples, respectively, and ϵ is the numerical stability constant.

Metrol. Meas. Syst., Vol. 30 (2023), No. 1, pp. 83–97
DOI: 10.24425/mms.2023.144394

2.2.3. Activation layer

An activation layer empowers the network to acquire a non-linear expression of the input signal to improve the capacity for representation and make the acquired features more separable using an activation function. The ReLU activation function is utilized in this work because it is quicker than alternative activation functions and does not have gradient vanishing issues [22]. The ReLU activation function may be represented as follows

$$f(x) = \begin{cases} x, & x \geq 0 \\ 0, & x \leq 0 \end{cases}, \tag{6}$$

where x is the output of the batch normalization layer and $f(x)$ is the activation of x.

2.2.4. Pooling layer

Typically, the pooling layer is positioned between two convolution layers that follow one another. Its purpose is to lower the size and quantity of trainable parameters for a CNN. The following equation can express the pooling transformation:

$$x_j^{l+1} = p\left(x_j^l\right), \tag{7}$$

where, $p(x_j^l)$ indicates the pooling operation and x_j^{l+1} is j-th feature of the $l+1$ layer. This work uses the max-pooling function which chooses the maximum of the restricted region as a feature input for the subsequent layers.

2.2.5. Fully connected layer

A traditional feed-forward neural network is employed in the fully connected layer of a CNN, which is used for classification. The output employs the softmax function as an activation function. The process of the fully connected layer is given as:

$$x^l = f\left(w^l x^{l-1} + b^l\right) \tag{8}$$

where f is the activation function, w^l and b^l are the weight and bias of the fully connected layer, respectively. The layer uses softmax as the activation function and is expressed as follows:

$$\sigma\left(z_j\right) = \frac{e^{zj}}{\sum_{k=1}^{K} e^{zk}}, \tag{9}$$

where e^{zk} is the exponential function enforced to the input vector, zj is the input vector, and k is the number of classes in the classification.

The architecture of the CNN used in this work is shown in Fig. 2. The input layer is 128×128×3 pixels in size, with 3 denoting a colourful image. All convolutional layers' kernels are of size 5×5. In the first convolution layer, 32 kernels are used, followed by 64 kernels in the second convolution layer and 128 kernels in the third convolution layer. The suggested CNN offers a batch normalizing layer following each convolution layer. The ReLU activation function is used in the suggested CNN, which speeds it up and lessens the vanishing gradient issue. After each activation layer, the max-pooling layer of size 2×2 and stride 2 is applied. The CNN uses four completely connected layers with 1000, 500, 100, and 5 neurons each. There is a softmax layer used before the classification layer.

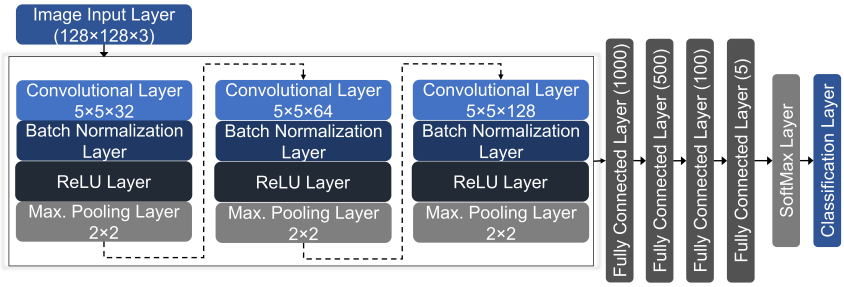

Fig. 2. Proposed architecture of the CNN.

3. Experimental studies

3.1. Description of the experimental setup

An experimental setup to simulate the effect of compound faults was established to prove the effectiveness of the proposed approach, as shown in Fig. 3.

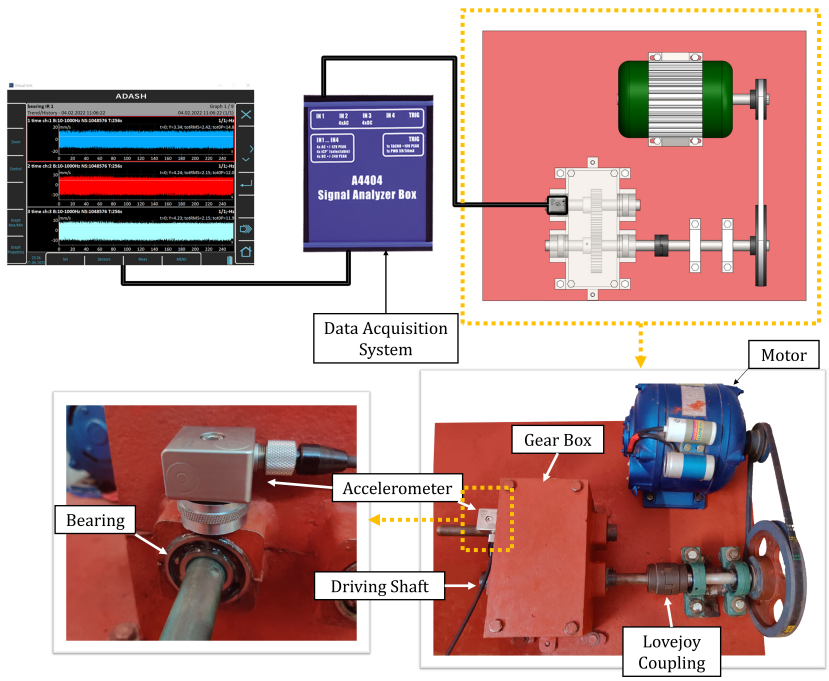

Fig. 3. Experimental setup.

The system has a single-stage spur gearbox and transmits the power from a motor of 0.5hp to a gearbox through a belt drive. SAE 40 oil is used as a lubricant in the gearbox. A piezoelectric accelerometer (CTC AC 115-1D) of 100 mV/g sensitivity is mounted on the bearing of the gearbox

Metrol. Meas. Syst., Vol. 30 (2023), No. 1, pp. 83–97
DOI: 10.24425/mms.2023.144394

to record the vibration signal. A signal conditioning unit is used to connect the accelerometer to a laptop. The details of gears and bearing are stated in Tables 1 and 2, respectively.

Table 1. Details of the gear and the pinion.

Parameters	Gear	Pinion
Number of teeth	40	20
Module	2.8 mm	
Pressure angle	20°	
Material	Mild steel	

Table 2. Details of the bearing.

Parameters	Details
Bearing number	SKF 6204
Pitch diameter	34.695 mm
Ball diameter	8 mm
Number of balls	8

3.2. Data acquisition

Two defective pinions and bearings are considered to measure the faulty systems' vibration response. A depth of 1 mm on either side of a tooth is removed along the flank face to represent the worn-out tooth, as illustrated in Fig. 4a).

The broken tooth gear was created by cutting a section of 9 mm in width and 2 mm in depth from the face of the gear tooth, as illustrated in Fig. 4b. The inner and outer race cracks in bearings are created using wire-cut EDM at a depth of 3 mm and a thickness of 0.2 5mm, as illustrated in Fig. 4c and d. The individual faults are combined to simulate the effect of compound faults, as listed in Table 3.

Table 3. Compound fault conditions.

Health Condition	Description
1	Healthy gear and bearing
2	Gear with a worn-out tooth and bearing with an inner race fault
3	Gear with a worn-out tooth and bearing with an outer race fault
4	Gear with a broken tooth and bearing with an inner race fault
5	Gear with a broken tooth and bearing with an outer race fault

A healthy gear and a healthy bearing were employed in Health Condition 1 to measure the vibration response of a fault-free system. In Health Condition 2, the healthy gear was replaced with a worn-out tooth gear, the healthy bearing was replaced with an inner race fault, and the vibration signals were recorded. Likewise, in Health Conditions 3, 4 and 5 the healthy gear and bearing were replaced with the defective ones, and the vibration signals were recorded. The motor speed and the sampling frequency for all health conditions was set to 540 rpm and 4096 Hz, respectively. Fig. 5 shows the raw vibration signals measured. Several trials were executed, and

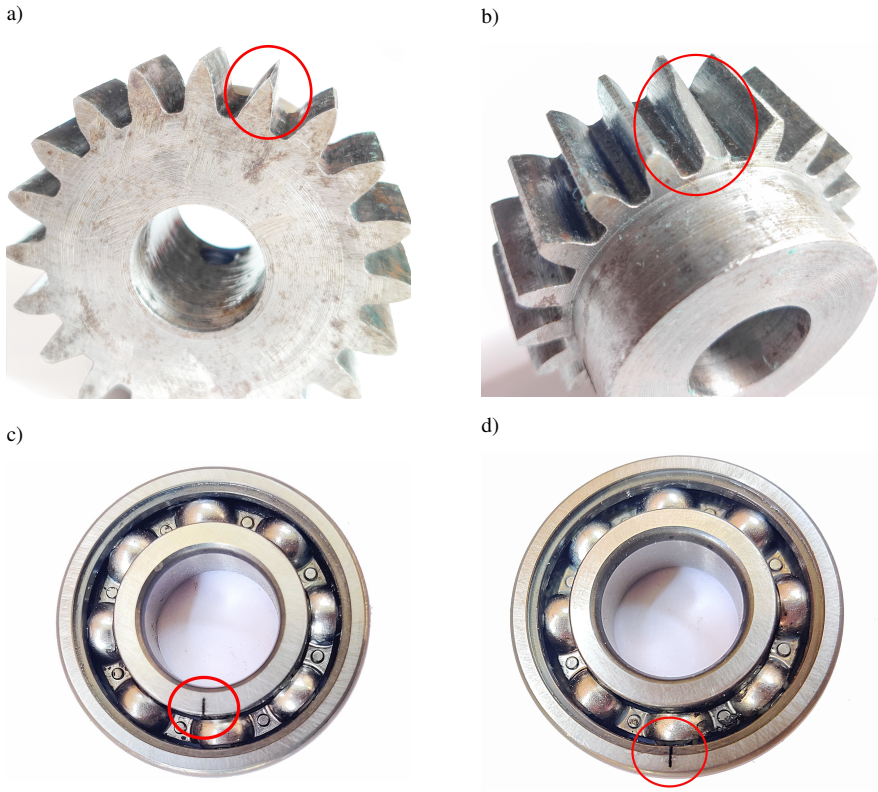

Fig. 4. Defective pinions and bearings: a) worn-out tooth, b) broken tooth, c) inner race fault, d) outer race fault.

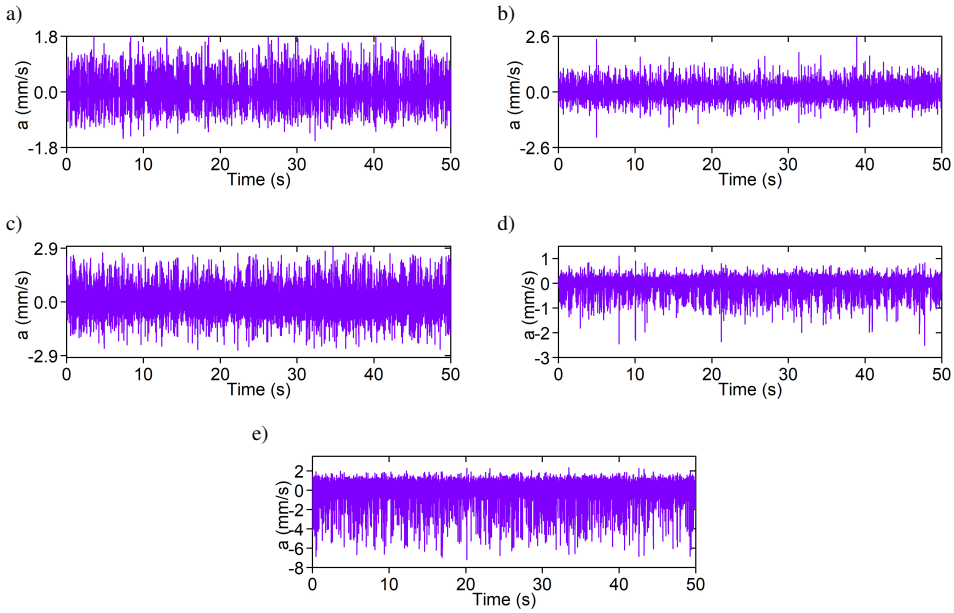

Fig. 5. Raw vibration signals: a) Condition 1, b) Condition 2, c) Condition 3, d) Condition 4, e) Condition 5.

Metrol. Meas. Syst., Vol. 30 (2023), No. 1, pp. 83–97
DOI: 10.24425/mms.2023.144394

the raw vibration signals were recorded. The recorded vibration signals were then sliced with overlap to enrich the training samples in each condition. Each sample had 1024 data points, while the training samples had an overlap of 512 data points.

4. Results and discussion

The Bessel Transform was employed to convert the time domain signal into TFD. For each condition, 400 TFD images were extracted and saved for analysis. Examples of Bessel-TFD images for all the Health Conditions are given in Fig. 6. In Health Condition 1, the operating frequency (F_o) is where the highest energy density is seen, as seen in Fig. 6a. As indicated in Figs. 6b and 6d, the highest energy density in Conditions 2 and 4 is observed at the Gear Mesh frequency (F_g), bearing inner race fault frequency (F_{bi}), and its harmonics. In the case of Health Conditions 3 and 5, as indicated in Fig. 6c and 6e, the most significant energy density is seen in the Gear Mesh frequency (F_g), bearing outer race fault frequency (F_{bo}), and its harmonics.

The details of training, validation and testing data are specified in Table 4. At the next stage holdout validation and testing were performed. 80% of the total images were used for training, 10% for validation, and 10% for testing the CNN. During the training process, the layers were set as displayed in Fig. 2. Three sets of convolutional layers, batch normalization layers, ReLU activation layers, maximum pooling layers and four fully connected layers were used. Finally, a softmax layer was used before the classification layer. The initial learning rate was set to 0.001, the maximum number of epochs was 100, and the validation frequency was 10. The Adam stochastic optimization algorithm was used to reduce the loss function. Five trials were executed, and the mean accuracy was considered as the concluding result.

Table 4. Details of the dataset.

Health Condition	Training Images (80%)	Validation Images (10%)	Testing Images (10%)
1	320	40	40
2	320	40	40
3	320	40	40
4	320	40	40
5	320	40	40
Total	1600	200	200

The training and validation accuracy of Trial 1 is shown in Fig. 7a and 7b. A final training accuracy of 100% and a validation accuracy of 97% were obtained in this trial. Further, the training loss and the validation loss for Trial 1 are shown in Fig. 7c and 7d. A final training loss of 8.09E-05 and a validation loss of 0.128 was obtained in Trail 1. Finally, the average validation accuracy for 5 trials was 96%.

The confusion matrix for trial 1 is illustrated in Fig. 8. The testing was conducted for all trails using the testing images after the training had been complete. In Trial 1, a testing efficiency of 95% was attained, and average testing efficiency of 94% was attained after five trials.

Further, the comparison of the proposed method with other TFDs is given in Fig. 9a and 9b. With all the TFDs, the CNN was applied with the same architecture and hyperparameters to find the validation and testing accuracies. Compared to the CWT, CQT, and SPWVD, the suggested Bessel transform-based technique has higher validation and testing accuracy for compound gear-bearing fault diagnosis.

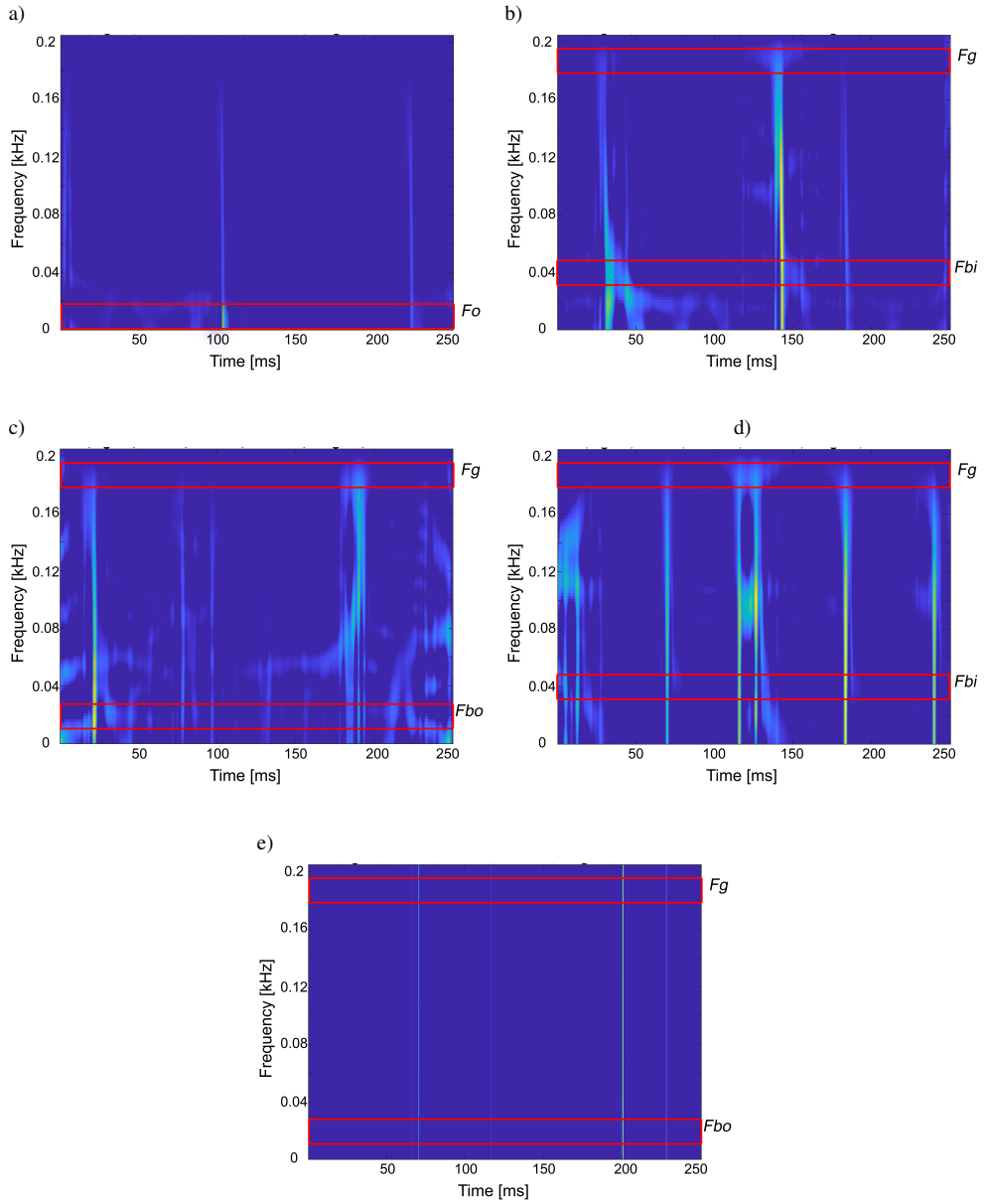

Fig. 6. Bessel-TFD of the vibration signals: a) Condition 1, b) Condition 2, c) Condition 3, d) Condition 4, e) Condition 5.

Hence, in the time-frequency domain, a suitable kernel function could be used to produce a time-frequency distribution with the desired properties. Further, using a time-frequency smoothing kernel function is crucial to suppress the cross-terms. As the cross-terms are successfully neglected with the Bessel transform while maintaining the auto terms with high precision, the performance of the Bessel transform is higher than that of the other transforms.

Metrol. Meas. Syst., Vol. 30 (2023), No. 1, pp. 83–97
DOI: 10.24425/mms.2023.144394

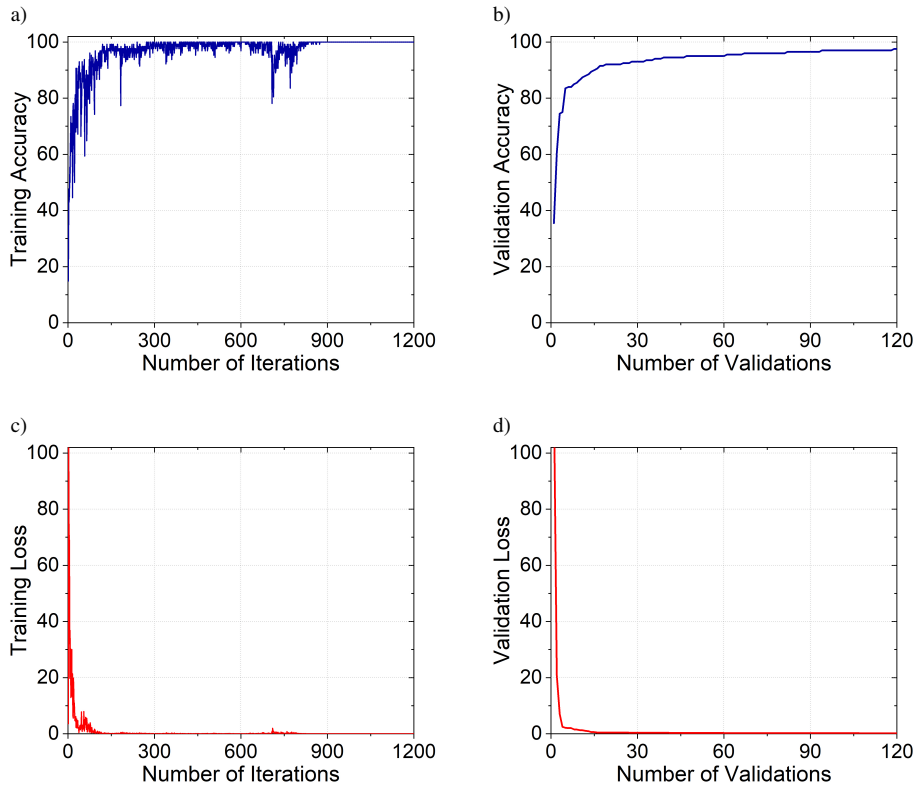

Fig. 7. Performance of trial 1: a) training accuracy, b) validation accuracy, c) training loss, d) validation loss.

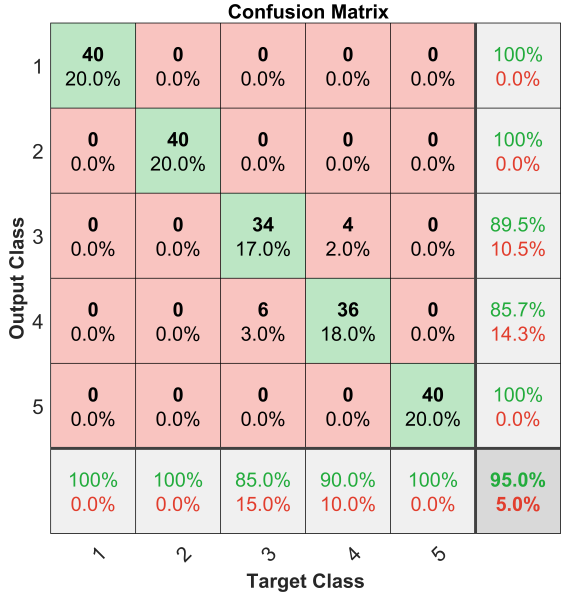

Fig. 8. Confusion matrix of testing results in Trial 1.

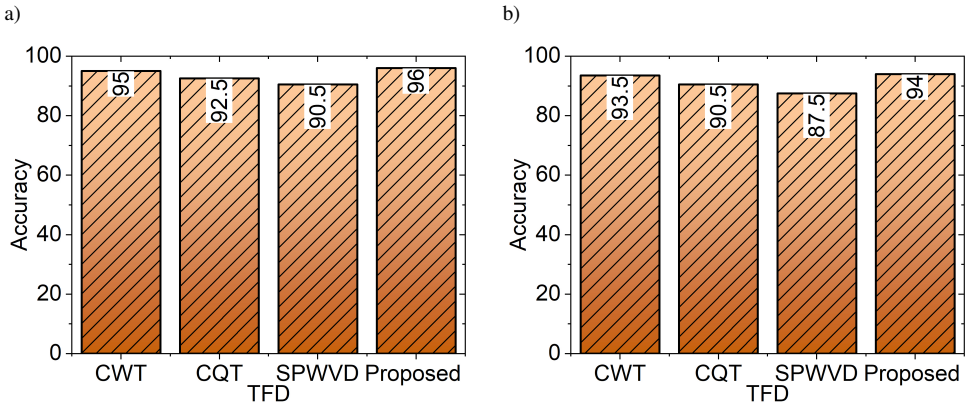

Fig. 9. Comparison of accuracies: a) Validation, b) Testing.

5. Conclusions

This research proposed an intelligent compound gear-bearing fault identification approach through Bessel Kernel-Based Time-Frequency Distribution and Convolutional Neural Networks. The Bessel transform was used in the proposed approach to convert the unprocessed time-domain vibration signals into TFD images. The CNN was used as a classifier to identify the faults using the extracted images. In CNN, 80% of the total images were used for training, 10% for validation and 10% for testing. A case study was used to verify the proposed approach, and the proposed approach effectively identified the faults. An average testing efficiency of 94% was attained in CNN using the extracted images.

The effectiveness of the proposed approach in identifying the compound gear-bearing faults was then compared with the CWT, CQT and PSWVD-based fault identification. The proposed Bessel transform-based method outperforms the other approaches. The industry needs for this proposed approach are high since numerous systems are vulnerable to compound gear-bearing problems. The effectiveness of this method can be increased in the future by eliminating the noises present in the vibration signals using advanced decomposition algorithms.

References

[1] Jia, Y., Li, G., Dong, X. & He, K. (2021). A novel denoising method for vibration signal of hob spindle based on EEMD and grey theory. *Measurement: Journal of the International Measurement Confederation*, *169*, 108490. https://doi.org/10.1016/j.measurement.2020.108490

[2] Babouri, M. K., Djebala, A., Ouelaa, N., Oudjani, B. & Younes, R. (2020). Rolling bearing faults severity classification using a combined approach based on multi-scales principal component analysis and fuzzy technique. *The International Journal of Advanced Manufacturing Technology*, *107*, 4301–4316. https://doi.org/10.1007/s00170-020-05342-6

[3] He, Q. (2013). Time-frequency manifold for non-linear feature extraction in machinery fault diagnosis. *Mechanical Systems and Signal Processing*, *35*, 200–218. https://doi.org/10.1016/j.ymssp.2012.08.018

Metrol. Meas. Syst., Vol. 30 (2023), No. 1, pp. 83–97
DOI: 10.24425/mms.2023.144394

[4] Wang, D., Tse, P. W. & Tsui, K. L. (2013). An enhanced Kurtogram method for fault diagnosis of rolling element bearings. *Mechanical Systems and Signal Processing*, *35*, 176–199. https://doi.org/10.1016/j.ymssp.2012.10.003

[5] Chandra, N. H. & Sekhar, A. S. (2016), Fault detection in rotor bearing systems using time frequency techniques. *Mechanical Systems and Signal Processing*, 72–73, 105–133. https://doi.org/10.1016/j.ymssp.2015.11.013

[6] Ibrahim, G. R. & Albarbar, A. (2011). Comparison between Wigner-Ville distribution- and empirical mode decomposition vibration-based techniques for helical gearbox monitoring. *Proceedings of the Institution of Mechanical Engineers, Part C: Journal of Mechanical Engineering Science*, *225*(8), 1833–1846. https://doi.org/10.1177/0954406211403571

[7] Aharamuthu, K. & Ayyasamy, E. P. (2013). Application of discrete wavelet transform and Zhao-Atlas-Marks transforms in non stationary gear fault diagnosis. *Journal of Mechanical Science and Technology*, *27*, 641–647. https://doi.org/10.1007/s12206-013-0114-y

[8] Inturi, V., Sabareesh, G. R., Supradeepan, K. & Penumakala, P. K. (2019). Integrated condition monitoring scheme for bearing fault diagnosis of a wind turbine gearbox. *JVC/Journal of Vibration and Control*, *25*(12), 1852–1865. https://doi.org/10.1177/1077546319841495

[9] Chen, X., Cheng, G., Li, H. & Li, Y. (2017). Fault identification method for planetary gear based on DT-CWT threshold denoising and LE. *Journal of Mechanical Science and Technology*, *31*, 1035–1047. https://doi.org/10.1007/s12206-017-0202-5

[10] Bordoloi, D. J. & Tiwari, R. (2014). Support vector machine based optimization of multi-fault classification of gears with evolutionary algorithms from time-frequency vibration data. *Measurement: Journal of the International Measurement Confederation*, *55*, 1–14. https://doi.org/10.1016/j.measurement.2014.04.024

[11] N. Holighaus, M. Dorfler, G.A. Velasco, T. Grill, (2012). A Framework for Invertible, Real-Time Constant-Q Transforms, *IEEE Trans. Audio Speech Lang. Process.*, *21*(4), 775-778. https://doi.org/10.1109/tasl.2012.2234114

[12] Rajagopalan, S., Restrepo, J. A., Aller, J. M., Habetler, T. G. & Harley, R. G. (2008). Nonstationary motor fault detection using recent quadratic time-frequency representations. *IEEE Transactions on Industry Applications*, *44*, 735–744. https://doi.org/10.1109/TIA.2008.921431

[13] Fernandes, F. C. A., Spaendonck, R. L. C. Van & Burrus, C. S. (2003). A New Framework for Complex Wavelet Transforms. *IEEE Transactions on Signal Processing*, *51*(7), 1825–1837. https://doi.org/10.1109/TSP.2003.812841

[14] F. Michael Thomas Rex, Andrews A., Krishnakumari, A. & Hariharasakthisudhan, P. (2020). A Hybrid Approach for Fault Diagnosis of Spur Gears Using HU Invariant Moments and Artificial Neural Networks. *Metrology and Measurement Systems*, *27*(3), 451–464. https://doi.org/10.24425/mms.2020.134587

[15] Zhenyu Guo, Louis-Gilles Durand, & Howard C. Lee. (1994). The time-frequency Distributions of Nonstationary Signals Based on a Bessel Kernel. *IEEE Transactions on Signal Processing*, *42*, 1700–1707. https://doi.org/10.1109/78.298277

[16] Y. Qu, Y. Zhang, M. He, D. He, & C. Jiao. (2019). Gear pitting fault diagnosis using disentangled features from unsupervised deep learning. *Proceedings of the Institution of Mechanical Engineers, Part O: Journal of Risk and Reliability*, *233*(5), 719-730. https://doi.org/10.1177/1748006X18822447

[17] S. Ma, F. Chu, & Q. Han. (2019). Deep residual learning with demodulated time-frequency features for fault diagnosis of planetary gearbox under nonstationary running conditions. *Mechanical Systems and Signal Processing*, *127*(1), 190–201. https://doi.org/10.1016/j.ymssp.2019.02.055

[18] L. H. Wang, X. P. Zhao, J. X. Wu, Y. Y. Xie, & Y. H. Zhang. (2017). Motor Fault Diagnosis Based on Short-time Fourier Transform and Convolutional Neural Network. *Chinese Journal of Mechanical Engineering (English Edition)*, *30*(6), 1357–1368. https://doi.org/10.1007/s10033-017-0190-5

[19] I. I. E. Amarouayache, M. N. Saadi, N. Guersi, & N. Boutasseta. (2020). Bearing fault diagnostics using EEMD processing and convolutional neural network methods. *International Journal of Advanced Manufacturing Technology*, *107*(9–10), 4077–4095. https://doi.org/10.1007/s00170-020-05315-9

[20] Y. Zhang, T. Zhou, X. Huang, L. Cao, & Q. Zhou. (2020). Fault diagnosis of rotating machinery based on recurrent neural networks. *Measurement: Journal of the International Measurement Confederation*, *171*, 108774. https://doi.org/10.1016/j.measurement.2020.108774

[21] Y. Gu, L. Zeng, & G. Qiu. (2020). Bearing fault diagnosis with varying conditions using angular domain resampling technology, SDP and DCNN. *Measurement: Journal of the International Measurement Confederation*, *156*, 107616. https://doi.org/10.1016/j.measurement.2020.107616

[22] S. K. Gundewar & P. V Kane. (2022). Bearing fault diagnosis using time segmented Fourier synchrosqueezed transform images and convolution neural network. *Measurement*, *203*, 111855. https://doi.org/10.1016/j.measurement.2022.111855

[23] T. Jin, C. Yan, C. Chen, Z. Yang, H. Tian, & S. Wang. (2021). Light neural network with fewer parameters based on CNN for fault diagnosis of rotating machinery. *Measurement*, *181*, 109639. https://doi.org/10.1016/j.measurement.2021.109639

[24] K. Su, J. Liu, & H. Xiong. (2021). Knowledge-Based Systems Hierarchical diagnosis of bearing faults using branch convolutional neural network considering noise interference and variable working conditions. *Knowledge-Based Systems*, *230*, 107386. https://doi.org/10.1016/j.knosys.2021.107386

[25] W. Zhang, C. Li, G. Peng, Y. Chen, & Z. Zhang. (2018). A deep convolutional neural network with new training methods for bearing fault diagnosis under noisy environment and different working load. *Mechanical Systems and Signal Processing*, *100*, 439–453. https://doi.org/10.1016/j.ymssp.2017.06.022

[26] Shao, H., Lin, J., Zhang, L. & Wei, M. (2020). Compound fault diagnosis for a rolling bearing using adaptive DTCWPT with higher order spectra. *Quality Engineering*, *32*, 342–353. https://doi.org/10.1080/08982112.2020.1749654

[27] Dhamande, L. S. & Chaudhari, M. B. (2018). Compound gear-bearing fault feature extraction using statistical features based on time-frequency method. *Measurement*, *125*, 63–77. https://doi.org/10.1016/j.measurement.2018.04.059

[28] Ou, L. & Yu, D. (2016). Compound fault diagnosis of gearboxes based on GFT component extraction. *Measurement Science and Technology*, *27*, 115007. https://doi.org/10.1088/0957-0233/27/11/115007

[29] A. Dibaj, M. M. Ettefagh, R. Hassannejad, & M. B. Ehghaghi. (2021). A hybrid fine-tuned VMD and CNN scheme for untrained compound fault diagnosis of rotating machinery with unequal-severity faults. *Expert Systems with Applications*, *167*, 114094. https://doi.org/10.1016/j.eswa.2020.114094

[30] Juan Xu, Long Zhou, Weihua Zhao, Yuqi Fan, Xu Ding & Xiaohui Yuan. (2022). Zero-shot learning for compound fault diagnosis of bearings. *Expert Systems with Applications*, *190*, 116197. https://doi.org/10.1016/j.eswa.2021.116197

Metrol. Meas. Syst., Vol. 30 (2023), No. 1, pp. 83–97
DOI: 10.24425/mms.2023.144394

[31] R. Huang, J. Li, W. Li and L. Cui. (2020). Deep Ensemble Capsule Network for Intelligent Compound Fault Diagnosis Using Multisensory Data. *IEEE Transactions on Instrumentation and Measurement*, *69*, 2304–2314. https://doi.org/10.1109/TIM.2019.2958010

[32] R. Huang, Y. Liao, and S. Zhang. (2019). Deep Decoupling Convolutional Neural Network for Intelligent Compound Fault Diagnosis. *IEEE Access*, *7*, 1848–1858. https://doi.org/10.1109/ACCESS.2018.2886343

[33] R. Huang, Z. Wang, J. Li, J. Chen and W. Li. (2020). A Transferable Capsule Network for Decoupling Compound Fault of Machinery. *2020 IEEE International Instrumentation and Measurement Technology Conference*, 1–6. https://doi.org/10.1109/I2MTC43012.2020.9129078

[34] R. Huang, J. Li, Y. Liao, J. Chen, Z. Wang and W. Li. (2021). Deep Adversarial Capsule Network for Compound Fault Diagnosis of Machinery Toward Multidomain Generalization Task. *IEEE Transactions on Instrumentation and Measurement*, *70*, 3506311. https://doi.org/10.1109/TIM.2020.3042300

[35] L. Cui, Y. Sun, J. Zhang, and H. Wang. (2021). Adapted dictionary-free orthogonal matching pursuit and 0-1 programming to solve the isolation and diagnosis of bearing and gear compound faults. *Measurement*, *178*, 109331. https://doi.org/10.1016/j.measurement.2021.109331

[36] B. Zhong, M. Zhao, S. Zhong, L. Lin, and L. Wang. (2022). Mechanical compound fault diagnosis via suppressing intra-class dispersions: A deep progressive shrinkage perspective. *Measurement*, *199*, 111433. https://doi.org/10.1016/j.measurement.2022.111433

[37] P. V. Shinde and R. G. Desavale. (2022). Application of dimension analysis and soft competitive tool to predict compound faults present in rotor-bearing systems. *Measurement*, *193*, 110984. https://doi.org/10.1016/j.measurement.2022.110984

[38] Cohen, L. (1989). Time-frequency distributions – a review. 941–981. *Proceedings of the IEEE*, *77*(7), 941–981. https://doi.org/10.1109/5.30749

Andrews Athisayam received his M.E in Engineering Design from Anna University, Chennai, India, in 2016. He is currently a Ph.D. candidate at the Department of Mechanical Engineering of the same university. His current research interests are vibration analysis and intelligent fault diagnosis of rotating machinery.

Manisekar Kondal receieved his Ph.D in metal forming from Manonmaniam Sundaranar University, Tirunelveli, India, in 2005. He is currently a Professor at the Department of Mechanical Engineering, National Engineering College, Kovilpatti, India. His research areas include fault diagnosis, tribology and composite materials. He has authored more than 50 papers.